Analysis of *NN* amplitudes up to 2.5 GeV: An optical model and geometric interpretation

H. V. von Geramb,[1,2] K. A. Amos,[1] H. Labes,[2] and M. Sander[2]
[1]*School of Physics, University of Melbourne, Parkville 3052, Australia*
[2]*Theoretische Kernphysik, Universität Hamburg, Luruper Chaussee 149, D-22761 Hamburg, Germany*
(Received 11 March 1998)

We analyze the SM97 partial wave amplitudes for nucleon-nucleon (*NN*) scattering to 2.5 GeV, in which resonance and meson production effects are evident for energies above the pion production threshold. Our analyses are based upon boson exchange or quantum inversion potentials with which the subthreshold data are fit perfectly. Above 300 MeV they are extrapolations, to which complex short-ranged Gaussian potentials are added to form a complex optical model potential. The data to 2.5 GeV are all well fit. The energy dependences of these Gaussians are very smooth save for precise effects caused by the known Δ and $N^{\star}$ resonances. With this optical model approach, we confirm that the geometrical implications of the profile function found from diffraction scattering are pertinent for the geometrical interpretation of the optical model absorption in the regime 300 MeV to 2.5 GeV. The overwhelming part of meson production comes from the QCD sector of the nucleons when they have a separation of their centers of 1 to 1.2 fm. [S0556-2813(98)00110-1]

PACS number(s): 13.75.Cs, 21.30.−x, 13.60.Le

I. INTRODUCTION

The nucleon-nucleon (*NN*) interaction at low and medium energy is a timely topic given the experimental efforts being made at institutions such as IUCF, TRIUMF, SATURN, CELSIUS, and COSY. It is a timely topic also theoretically given the plethora of models of *NN* scattering in vogue. Below the pion threshold (which we take to be synonymous with 300 MeV throughout this paper), the phenomenology is rather simple as empirically there is only the deuteron bound state, the elastic scattering and $NN\gamma$ bremsstrahlung. For this domain of energies below 300 MeV, there exist excellent experimental data and several potential models whose parametrizations give fits with $\chi^2 \sim 1$. There have been many fine presentations of the experimental [1,2] and theoretical [3,4] developments for this energy regime also.

Above the pion threshold, the experimental situation is excellent also [1]. But as there are many inelastic channels, the available experimental information is less complete. Nevertheless, in the energy regime 300 MeV to 1 GeV, a number of experiments have produced data of such quality that existing models of *NN* scattering are severely tested. The models predicated upon quality fits to *NN* scattering data below the pion threshold have to be modified if they are to be used as a starting point for analyses of the higher-energy data. Notably they must be varied to account for the various meson production thresholds and also to account for effects of known resonance structures in the *NN* system. Of the latter, the Δ and N^* are the relevant entities for the energy range considered, and the effects resulting from interference of their associated scattering amplitudes with those of other possible scattering processes are very evident in the structures of the cross-section data and spin observables. Those effects are not severely localized in energy as the resonances have large widths for the decay. Indeed, amplitudes for $N\Delta$, NN^*, $\Delta\Delta$ among others are important and affect *NN* scattering at all energies in the range from threshold to over 2 GeV. Some of the studies of these problems based upon boson exchange models give qualitative if not quantitative descriptions of the situation [5–10]. Lomon [11] has studied such resonance phenomena in a different way by using a boundary condition model.

In the energy range above 5 GeV, the *NN* scattering system is one of many overlapping resonances and many open reaction channels. A consequence is that diffraction models, such as epitomized by Glauber or Regge theories [12], explain very well the measured total and soft interaction *NN* scattering cross sections from about 5 GeV to the highest experimental energy [13–16]. As the energy decreases to around 2 GeV, a more specific treatment of the scattering process is needed to explain observation. An optical model approach by Neudatchin *et al.* [17] so far has covered the entire energy range below 6 GeV and they found reasonable agreement with data. But there was little data for high precision phase shift analyses available for use with their analysis and they did not seek fits to data that qualify also as high precision. In fact, then essentially phase shift values to 1 GeV only were known with some confidence [1]. This situation has changed drastically in the intervening years. Recently Arndt *et al.* [18] have investigated elastic scattering data for energies up to 2.5 GeV and they have defined partial wave scattering amplitudes which are available from SAID [19], as are a wide range of other options.

A key feature in all studies of partial wave amplitudes has been the attributes of the chosen phase shift specifications. Until recently the data to 300 MeV led to diverse solutions from various groups [1,20,21]. Qualitatively they obtain the same results to 300 MeV with the exception of the $^1P_1$ channel and the mixing angle ϵ_1. Inclusion of extra data sets (to 1 GeV) in an extension of the method of analysis [1,2,20] helped resolve some of that ambiguity. New data then extended the range of the analysis to 1.6 GeV [1], from which a confident solution for the amplitudes was defined to about 1.2 GeV. Finally, the data from COSY pushed that limit to 2.5 GeV with a confidence interval to about 1.75 GeV [18]. A noted result of this most recent development is that the *NN* partial wave amplitudes are particularly smooth functions of energy allowing for large width resonance structures

associated with Δ (1232 MeV) and N^* (1440 MeV) formation. The essentially smooth behavior of the scattering amplitudes was not anticipated. There were expectations that dibaryon resonances effects would exist as well [22,23,11]. If such do exist in the range to 1.8 GeV, then either they must have very small coupling strengths or they must have very narrow or extremely large widths.

The character of the scattering amplitudes up to 2.5 GeV is consistent with the optical potential concept. Thus we suggest a potential approach to the analyses of that data based upon extrapolating a high precision *NN* interaction, established by its fit to data below 300 MeV, to energies above that and correcting with energy-dependent optical potentials in each partial wave. By so doing, we account for the spin, isospin, and momentum dependences of underlying boson exchange mechanisms. At the highest energy, as so many partial wave amplitudes contribute to scattering, the optical potential scheme should simplify and ultimately merge to the optical disc of diffraction models. A consequence of this approach is a geometric picture of *NN* scattering from the highest energies down; a picture which has been correlated to the Regge theory with Pomeron exchanges [13–16].

Our theoretical efforts to analyze *NN* data to 2.5 GeV, begins either with boson exchange models, in particular the nonlinear one solitary boson exchange potential (OSBEP), or quantum inversion. Observed data in the subthreshold region <300 MeV are reproduced perfectly by those two very different approaches with OSBEP defining a potential in momentum space while inversion leads to a local coordinate space one [24,25]. As we indicated above, use of these potentials as well as of the Paris [26], Nijmegen [27], AV18 [28], and Bonn-CD [29] potentials for energies above 300 MeV are extrapolations. They all give similar results and could be used as a real background potential in an extended application to account for meson exchanges for energies >300 MeV. For energies above 300 MeV, our model is to add to any of the background potentials, a real and imaginary potential with Gaussian form factors whose parameters are adjusted to give fits to the SM97 partial wave amplitudes [18]. Smooth energy-dependent results have been found that are consistent with the structures in the SM97 data, which indicate resonances in several partial waves, notably the $P_{33}(1232)$ and $P_{11}(1440)$, on an otherwise smooth energy-dependent background. The optical potentials are complex and short ranged typically of nucleon size that is known from analyses of electron scattering off a nucleon. This implies the first of our conjectures that production processes are localized at and within the confinement surface of a nucleon. The results we display also supports our second conjecture that the geometry of the profile function, known from high-energy diffraction scattering, remains valid at lower energies and especially in the P_{33} and P_{11} resonance dominated region. It is this result that lead us to expect also that meson production is a unique QCD aspect applicable from threshold (300 MeV) up to highest energies.

In Sec. II, the basis and form of the optical potential we investigate for *NN* scattering above threshold is defined. The results of our calculations then are given in Sec. III and the geometric picture we associate with them is presented in Sec. IV. Finally a summary of this work and the conclusions we have drawn from our results are presented in Sec. V.

II. OPTICAL POTENTIAL—ITS BASIS AND FORM

To describe *NN* scattering, we adopt a coordinate space view. At very long range, electromagnetic interactions alone are important, but as the range decreases, boson exchange attributes become increasingly effective. The onset is at about 15 fm with the exchange of a pion. As the range shortens further, then σ, ρ, ω meson and baryon exchanges add in. At the shortest distances, inside 0.8 fm typically, all *NN* potentials have strong repulsion. The precise character of this core is not a sensitive quantity, so far as low- to medium-energy *NN* scattering is concerned. Past success of the use of soft and hard core potentials reflects that lack of sensitivity.

The boson exchange models which we ascribe to the medium- and long-range attributes, are developed in momentum space. The associated interactions are nonlocal. With reasonable values for the meson-nucleon coupling constants and form factor cutoffs, these boson exchange models give quality fits to the data that lead to their nomination as high precision interactions [4,27–29,24]. That is also the case with other approaches such as those with explicitly momentum-dependent potential models [26,27], energy-independent partial wave potential models [25,27,28], and, with somewhat different approaches, the Moscow potential model [30] and the MIT boundary condition model [11]. These approaches are motivated differently in their formulation but in the end all give essentially the same on-shell *NN* *t* matrices below threshold.

We are particularly interested in those potentials obtained by use of inverse scattering theories that are predicated upon a Schrödinger equation as the equation of motion. This is an ill-posed problem since only discrete data with uncertainties in the finite interval 0 to 300 MeV are input. Solution of the inverse problem then requires an interpolation and an extrapolation of the data. We constrain that extrapolation so that the *S* matrix remains unitary at all energies. Below the pion threshold this is a very good approximation since bremsstrahlung is the only open channel and, as that has a small cross section, it is customary to neglect this violation of unitarity. The problem then is well-posed and, by using Gel'fand-Levitan-Marchenko equations, real and energy-independent inversion potentials have been constructed partial wave by partial wave [25,31,32]. By dint of this construction the on-shell *t* matrices (0 to 300 MeV) are perfectly reproduced.

In recent years, attempts have been made to discern between these diverse model views by seeking explicit effects in data due to the off-shell properties of the associated *NN* *t* matrices. Studies of three nucleon systems, of bremsstrahlung, and in microscopic nucleon-nucleus optical models are examples. So far no study has been able to discriminate one model form over any other or even set a preference order. While all of the potential models considered are relevant physically only for the range 0 to 300 MeV, mathematically there is no prohibition in obtaining solutions for energies above threshold. The extrapolations are shown for several of these potentials in Figs. 1–4. The phase parameters correspond to the Arndt-Roper convention as described in the first cited article [1]. For any partial wave δ_{SLJ}, $\Delta\delta_{SLJ}$, ρ_{SLJ}, $\Delta\rho_{SLJ}$, and/or *T* matrices were retrieved with Basque option in the calling sequence. For uncoupled channels, we show

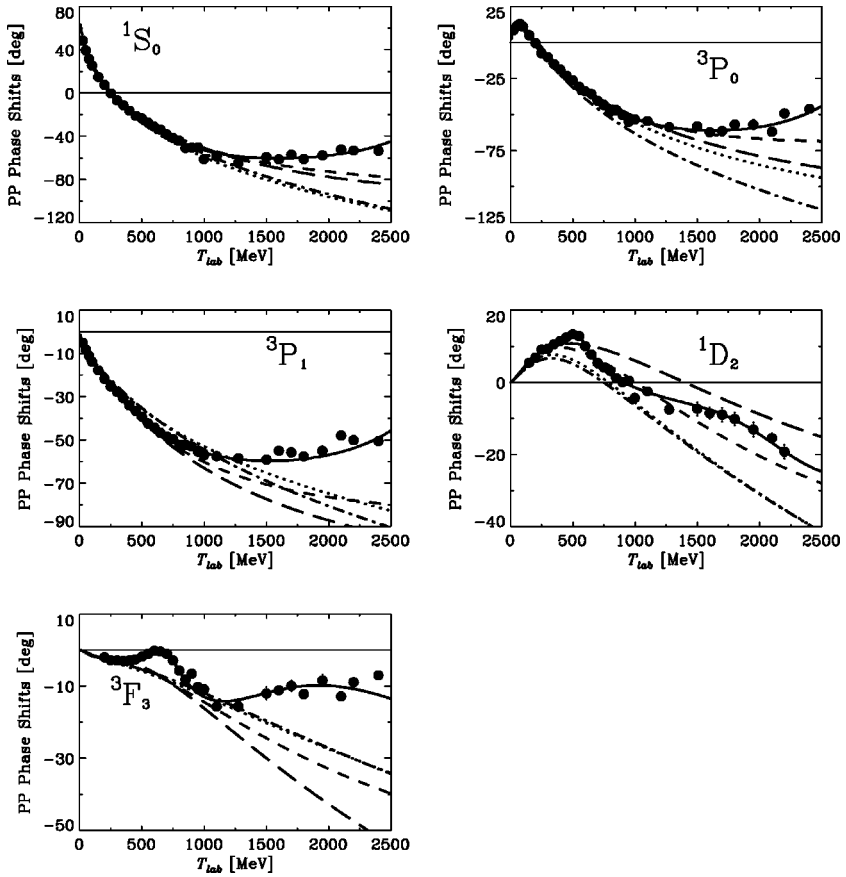

FIG. 1. The phase shifts for proton-proton scattering in uncoupled channels. The full dots are SM97 single energy fits while the solid curves represent the SM97 continuous energy fits as well as the final results of our optical model searches. These are compared with the results of the inversion potentials based upon SM94 values (dashed), the OSBEP (dash-dotted), the AV18 (long dashed), and the Bonn-B (dotted) results.

the resultant δ_{SLJ} in Figs. 1 and 3, and in Fig. 5 the associated $\eta_{SLJ}=|S_{SLJ}|$. For coupled channels the results we give in Figs. 2, 4 and 6. They are derived from the S matrix, which in turn is calculated from the SAID T matrix with $S=1+2iT$. This gives a somewhat better accuracy since the phase parameters δ, ϵ, ρ, and Φ are curtailed. The coupled channels absorption is shown for the diagonal elements, $\eta_{SLJ}=(S\cdot S^{\dagger})^{1/2}$. For pure elastic scattering the phase con-

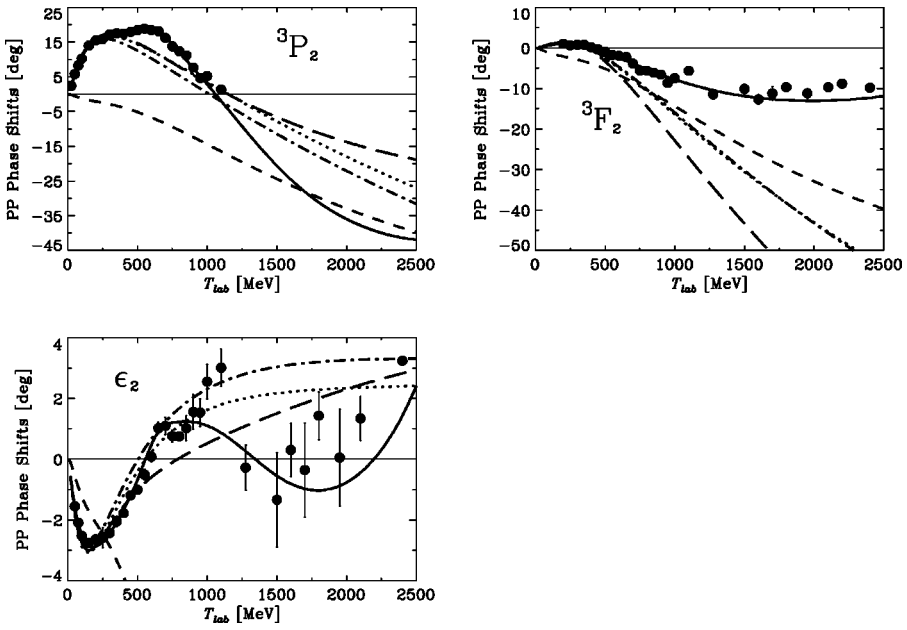

FIG. 2. The SYM phase shifts for proton-proton scattering in the $^3PF_2$ coupled channels. The nomenclature is as in Fig. 1.

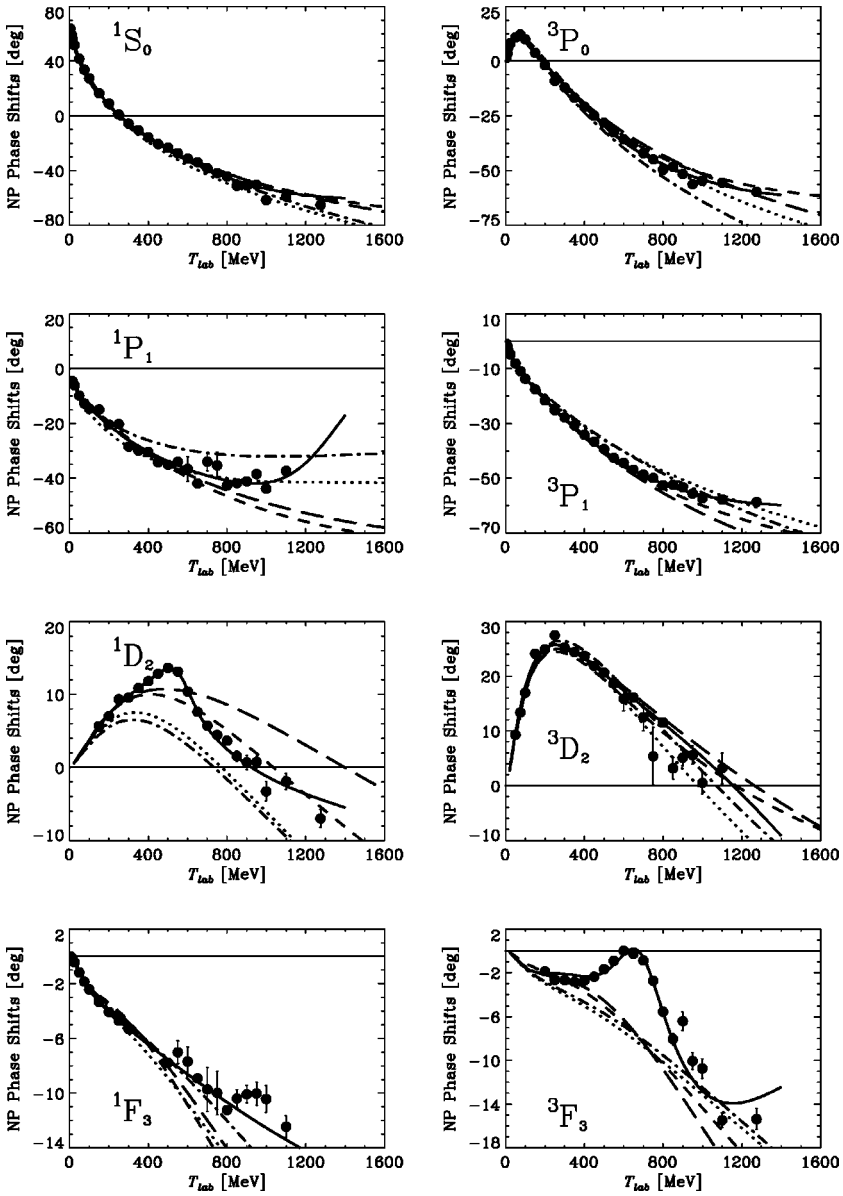

FIG. 3. The phase shifts for neutron-proton scattering in the single channels. The nomenclature is as in Fig. 1.

vention corresponds to Stapp, Ypsilantis, and Metropolis (SYM). Qualitatively they are similar in all channels save for those in which the known resonances have big effects; notably in $^1D_2$, $^3F_3$, and $^3PF_2$ channels. All of these potentials are purely real so that they result in unitary S matrices, as they do not incorporate production or annihilation of mesons; effects which are important in analyses of data above 300 MeV. This is evident in Figs. 5 and 6 in which the absorption is shown for proton-proton and neutron-proton channels, respectively.

There exist extensions to boson exchange models which incorporate particle production explicitly [5–10]. They reproduce well observed NN and $NN\pi$ data up to 1 GeV. At the time data above that energy were sparse. Even so, these calculations are extremely complex; much more so than for the boson exchange models that are their base. Also the number of adjustable parameters involved increase with every additional element in the theory. Most seriously from our point of view, however, is that the conventional boson exchange amplitudes are varied from the forms optimal below 300 MeV to have a perfect fit above 300 MeV. Consequently the NN potentials are affected at short- and medium-range radii and the meson production would not be as localized as we believe it to be. We conjecture that meson production is a genuine QCD effect and so, in a geometric view, emanate from the QCD bag. It is also the case that the partial wave amplitudes are very smooth functions of energy, giving credence to our view that a model with far fewer degrees of freedom should suffice. In light of the above, we seek a simpler phenomenological approach to interpret the elastic scattering and reaction cross sections above 300 MeV. It is the optical model. Use of complex optical potentials to analyze hadron-hadron scattering is not new [13]. Most studies also have shared the general characteristics of that optical potential by its links to the strong absorption model that works so well with high-energy scattering data. For NN scattering to 6 GeV, such an approach has been used recently as well [17]. But there now is quite excellent data to 2.5 GeV and there are diverse basic NN interactions that give high

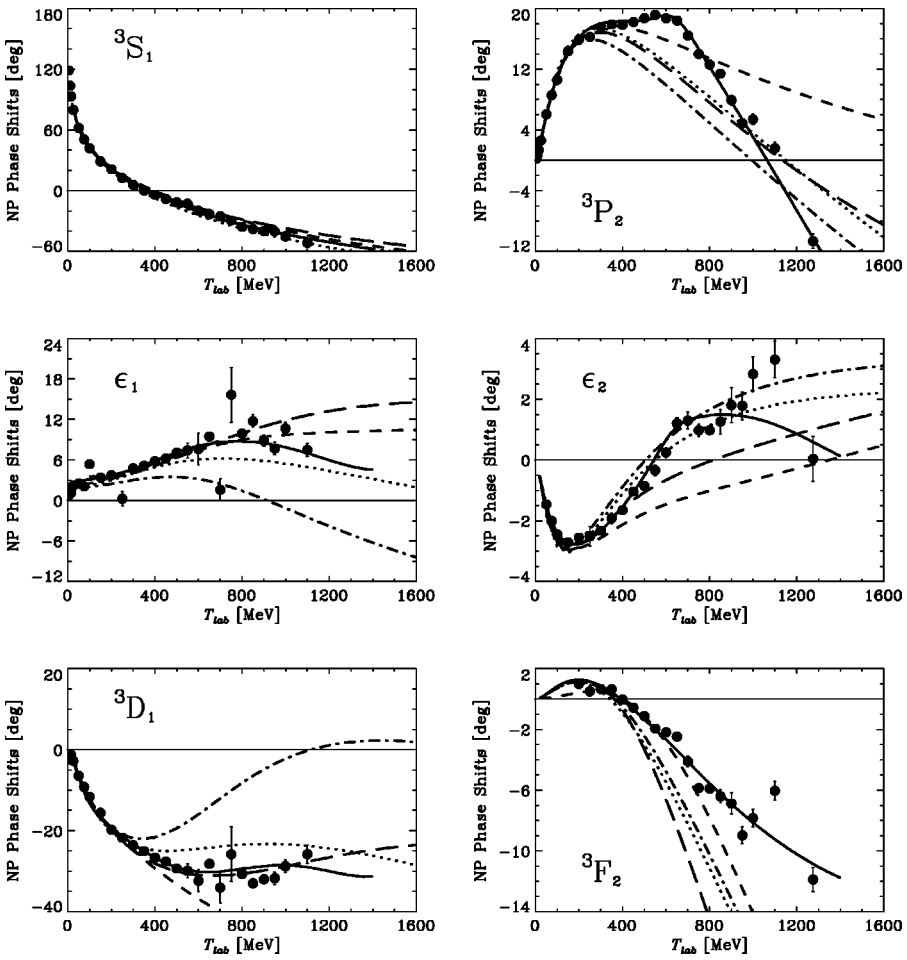

FIG. 4. The SYM phase shifts for neutron-proton scattering in the $^3SD_1$ and $^3PF_2$ coupled channels. The nomenclature is as in Fig. 1.

precision fits to subthreshold data for use as sensible background interactions.

The optical model for scattering is a concept that is well developed in nuclear physics from both a purely phenomenological view as well as from a microscopic (folding model) one. That is especially the case for nucleon scattering from nuclei with projectile energies to 400 MeV and more. The phenomenological approach was developed first as a means to categorize much data and the smooth behavior with energy, target mass, and projectile type of those nuclear optical potentials indicated a sensibility of the model and gross properties of nuclear systems which more fundamental approaches should encompass. The microscopic models of nucleon-nucleus scattering were developed subsequently. With them excellent results can now be obtained whether the approach is based on a model in momentum space [33] or on one in coordinate space [34]. The complex optical potentials predict nucleon-nucleus scattering that agree very well with measured cross sections and spin observables for all nuclei between ^{3}He and ^{238}U. These proton-nucleus optical model results correlate with intrinsic nuclear structure consistent with electron scattering form factors from those nuclei.

It may be argued that an optical model approach for study of *NN* scattering is not necessary as the extended boson exchange models will provide the essential information that a QCD based theory must emulate. For all the reasons listed above, this is not our opinion. Our use of an optical model approach to the analysis of *NN* scattering above pion threshold is predicated in part upon the successful use of that approach to proton-nucleus scattering analyses but also because of the folding to get the proton-nucleus optical potentials is similar in spirit to what has been proposed for quarks by Nachtmann *et al.* [35]. Also there is a synergy of optical potential methods between low-energy and high-energy scattering studies and we seek its form for *NN* scattering over the entire energy range. The criterion that we have a sensible result will be that of a smooth behavior of the properties of the potentials found and a consistent geometric interpretation of what the complex potentials reflect. We comment on this later but first we show that analyses made using a relativistic Schrödinger equation are pertinent.

It is generally accepted that a valid covariant description of *NN* scattering formally is given by the Bethe-Salpeter equation

$$\mathcal{M}=\mathcal{V}+\mathcal{V}\mathcal{G}\mathcal{M}, \tag{1}$$

where $\mathcal{M}$ are invariant amplitudes that are based upon irreducible diagrams as contained in $\mathcal{V}$ and $\mathcal{G}$ is a relativistic propagator. This equation serves generally as an ansatz for approximations. Of those, the three-dimensional reductions are of great use and, of those, the Blankenbecler and Sugar [36] reduction gives an equation that has received most attention for applications with *NN* scattering [37,4]. In this approach an effective potential operator is introduced which

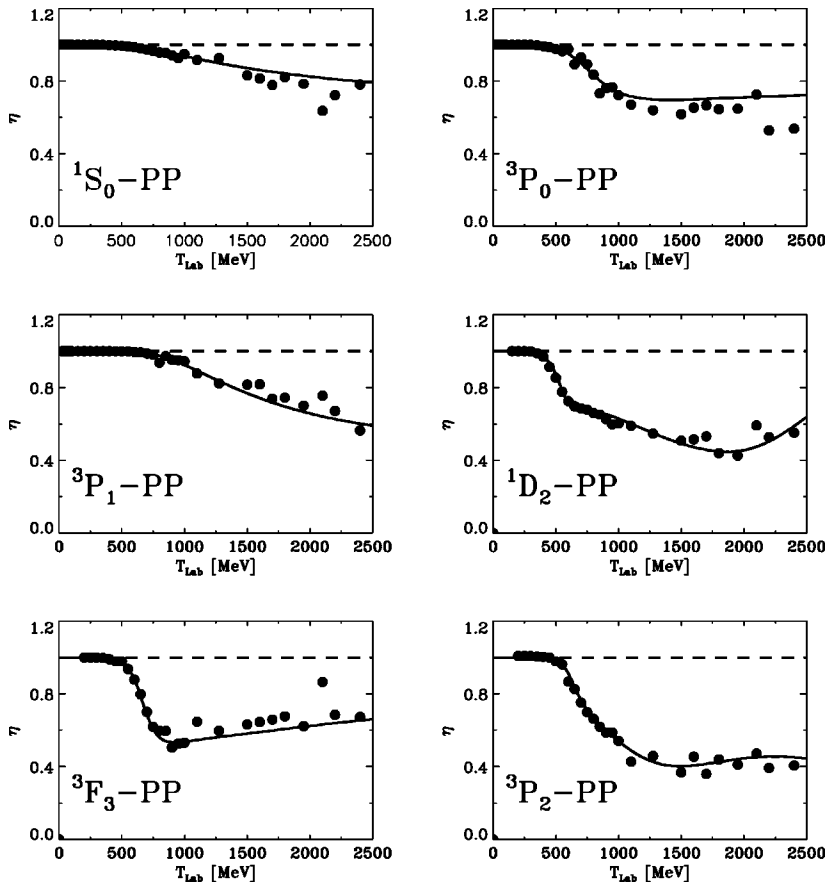

FIG. 5. The absorption $\eta=(S\cdot S^{\dagger})^{1/2}$ for proton-proton scattering. Channels with small absorptions, $1\geqslant\eta>0.98$, are not included. The full dots are SM97 single energy fits while the solid curves represent the SM97 continuous energy fits as well as the final results of our optical model searches. Models without imaginary potential do not produce any absorption, $\eta=1$ (dashed).

one identifies as the *NN* interaction potential. This reduction is obtained from the integral equation (1), which in terms of four-momenta [38] is

$$\mathcal{M}(q',q;P)=\mathcal{V}(q',q;P)+\int d^4k\mathcal{V}(q',k;P)\mathcal{G}(k;P)\mathcal{M}(k,q;P), \tag{2}$$

with the propagator

$$\mathcal{G}(k;P)=\frac{i}{(2\pi)^4}\left[\frac{(1/2)\not{P}+\not{k}+M}{[(1/2)P+k]^2-M^2+i\varepsilon}\right]^{(1)}\times\left[\frac{(1/2)\not{P}+\not{k}+M}{[(1/2)P+k]^2-M^2+i\varepsilon}\right]^{(2)}. \tag{3}$$

The superscripts refer to the nucleon (1) and (2), respectively, and in the c.m. system, $P=(\sqrt{s},0)$, with total energy $\sqrt{s}$. The Blankenbecler-Sugar reduction of the propagator $\mathcal{G}$ is to use the covariant form

$$\mathcal{G}_{\mathrm{BbS}}(k,s)=-\frac{\delta(k_0)}{(2\pi)^3}\frac{M^2}{E_k}\frac{\Lambda_+^{(1)}(\mathbf{k})\Lambda_+^{(2)}(-\mathbf{k})}{(1/4)s-E_k^2+i\varepsilon}, \tag{4}$$

where the positive energy projector is given as

$$\Lambda_+^{(i)}(\mathbf{k})=\left(\frac{\gamma^0E_k-\vec{\gamma}\cdot\mathbf{k}+M}{2M}\right)^{(i)}. \tag{5}$$

Then the three-dimensional equation

$$\mathcal{M}(\mathbf{q}',\mathbf{q})=\mathcal{V}(\mathbf{q}',\mathbf{q})+\int\frac{d^3k}{(2\pi)^3}\mathcal{V}(\mathbf{q}',\mathbf{k})\times\frac{M^2}{E_k}\frac{\Lambda_+^{(1)}(\mathbf{k})\Lambda_+^{(2)}(-\mathbf{k})}{\mathbf{q}^2-\mathbf{k}^2+i\varepsilon}\mathcal{M}(\mathbf{k},\mathbf{q}), \tag{6}$$

is obtained. Taking matrix elements with only positive energy spinors, an equation with minimum relativity is obtained for the *NN* t matrix, namely,

$$\mathcal{T}(\mathbf{q}',\mathbf{q})=\mathcal{V}(\mathbf{q}',\mathbf{q})+\int\frac{d^3k}{(2\pi)^3}\mathcal{V}(\mathbf{q}',\mathbf{k})\times\frac{M^2}{E_k}\frac{1}{\mathbf{q}^2-\mathbf{k}^2+i\varepsilon}\mathcal{T}(\mathbf{k},\mathbf{q}). \tag{7}$$

With the substitutions

$$T(\mathbf{q}',\mathbf{q})=\left(\frac{M}{E_{q'}}\right)^{1/2}\mathcal{T}(\mathbf{q}',\mathbf{q})\left(\frac{M}{E_q}\right)^{1/2} \tag{8}$$

and

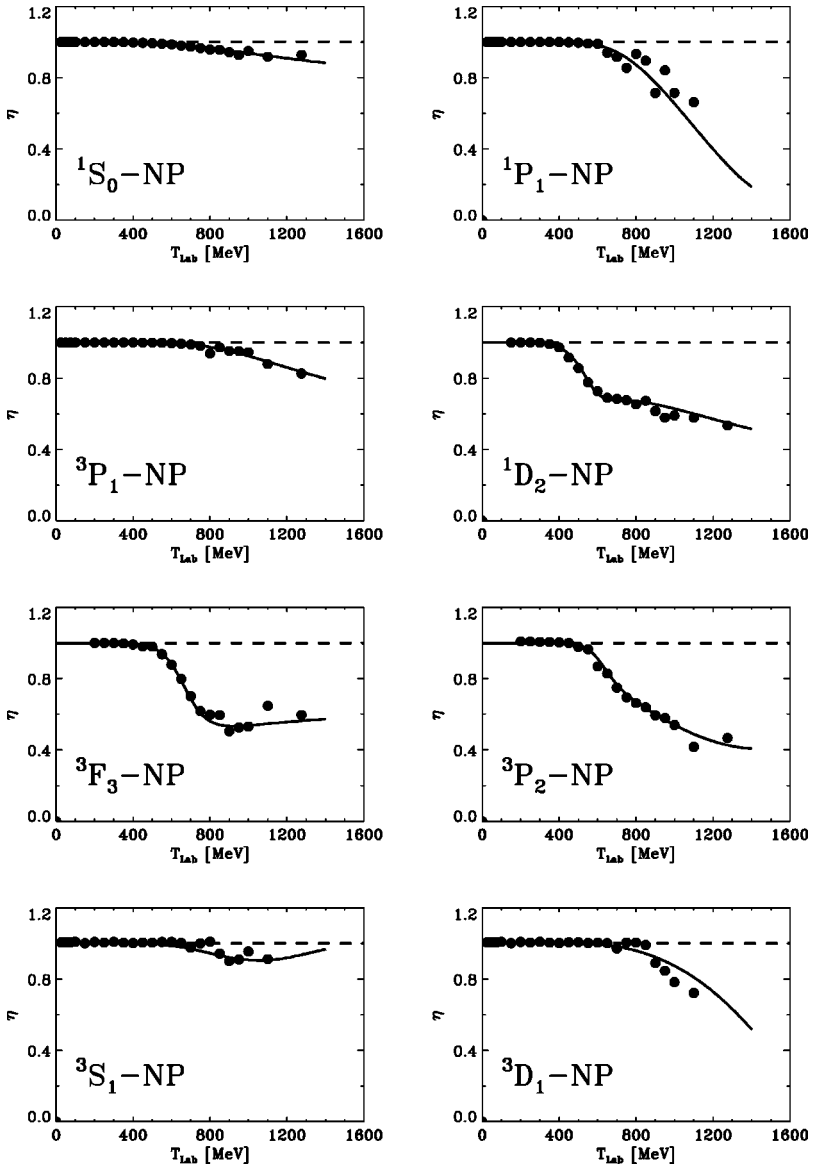

FIG. 6. Same as Fig. 5 but for neutron-proton channels. Consider $\eta(^3P_0-NP)\sim\eta(^3P_0-PP)$.

$$V(\mathbf{q}',\mathbf{q})=\left(\frac{M}{E_{q'}}\right)^{1/2}\mathcal{V}(\mathbf{q}',\mathbf{q})\left(\frac{M}{E_q}\right)^{1/2}, \tag{9}$$

we obtain an expression equivalent to the nonrelativistic Lippmann-Schwinger equation,

$$T(\mathbf{q}',\mathbf{q})=V(\mathbf{q}',\mathbf{q})+\int\frac{d^3k}{(2\pi)^3}V(\mathbf{q}',\mathbf{k})\,\frac{M}{\mathbf{q}^2-\mathbf{k}^2+i\varepsilon}T(\mathbf{k},\mathbf{q}). \tag{10}$$

This is equivalent to the Schrödinger equation in coordinate space

$$[-\Delta+MV(\mathbf{r})-k^2]\psi(\mathbf{r},k)=0, \tag{11}$$

where M is the reduced mass,

$$M=\frac{2\mu}{\hbar^2}=\frac{2}{\hbar^2}\frac{m_1m_2}{m_1+m_2}. \tag{12}$$

Because of the (M/E) factors in the transformation (9), an explicitly energy-independent potential $V(\mathbf{q}',\mathbf{q})$ becomes an energy-dependent one $\mathcal{V}(\mathbf{q}',\mathbf{q})$. We note that a proper relativistic wave equation would contain coupling to negative energy solutions also, but this we neglect. In the Schrödinger equation (11), k^2 should be calculated relativistically, so defining the relativistic Schrödinger equation which we have solved using an interaction of the form

$$V(\mathbf{r})\rightarrow V_{NN}+V_{OMP}(r,s)+iW_{OMP}(r,s)+\frac{e^2Z_1Z_2}{r}, \tag{13}$$

where V_{NN} is an energy-independent background potential and (V_{OMP},W_{OMP}) is an energy-dependent complex optical potential

$$V_{OMP}(r,s)=V_0(s)\exp(-r^2/a^2) \tag{14}$$

and

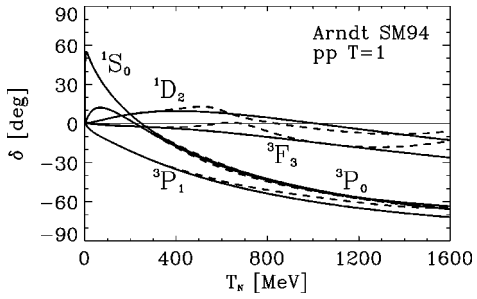

FIG. 7. The real phase shifts of SM94 for $T=1$ proton-proton scattering (dashed curves) compared to the phase shifts given from our inversion potentials (solid curves).

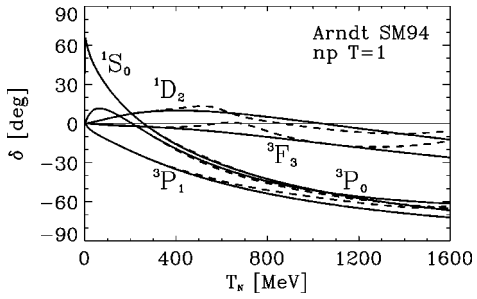

FIG. 8. The real phase shifts of SM94 for $T=1$ neutron-proton scattering (dashed curves) compared to the phase shifts given from our inversion potentials (solid curves).

$$W_{OMP}(r,s)=W_0(s)\exp(-r^2/b^2). \tag{15}$$

Our choice of Gaussian form factors for the optical potential is based in part upon the success of the Chou-Yang model [13] which shows that the charge form factor of the proton determines the momentum transfers in their approach. The proton charge form factor is very well represented by a Gaussian and folding two Gaussians yields again a Gaussian. For coupled channels, $V(\mathbf{r})$ in Eq. (13) becomes a 2×2 matrix. The optical potential search in this case is ambiguous if one uses the full matrix form, since the optical model then has to account for flux losses into the production channels as well as flux interchange between the coupled channels themselves. The best situation would be to suppress the possibility of flux interchanges between the explicitly included coupled channels but such is not feasible within a search. Thus we have estimated the optical potentials in coupled channel cases by using a two-step procedure. We run the coupled channel search twice with the optical potential matrix restricted to act in channel $^3S_1$ ($^3P_2$) and $^3D_1$ ($^3F_2$), respectively. The search criteria then were solely the diagonal S matrix elements of each channel in turn.

These equations are solved using partial wave expansions and so any of the coordinate space potentials could be used as the background, partial wave by partial wave. We use the inversion potentials since the inverse scattering approach always maps the latest phase shifts as accurately as one wishes and permits a controlled extrapolation above 300 MeV.

To complete the specifications of our solutions of the relativistic Schrödinger equations, we give the relevant kinematics. With m_1 being the projectile and m_2 the target nucleon, the Mandelstam variable s, and the invariant mass M_{12}, are given by

$$s=M_{12}^2=(m_1+m_2)^2+2m_2T_{\rm lab}=(\sqrt{k^2+m_1^2}+\sqrt{k^2+m_2^2})^2, \tag{16}$$

while the relative momentum in the c.m. system is

$$k^2=\frac{m_2^2(T_{\rm lab}^2+2m_1T_{\rm lab})}{(m_1+m_2)^2+2m_2T_{\rm lab}}, \tag{17}$$

which, for equal masses, reduces to

$$k^2=\frac{1}{4}s-m_1^2=\frac{1}{2}m_1T_{\rm lab}. \tag{18}$$

Integration of the partial wave components of Eq. (11) is achieved using the Numerov method to ascertain the asymptotic forms of the scattering solutions from which we get the phase shifts.

III. OPTICAL MODEL ANALYSES

First we consider the background potentials we have used in our optical model approach [31]. Given our primary interest in a geometric view of the scattering process, we seek background potentials that encompass the basic boson exchange processes as exactly as possible. This we define by virtue of a high precision fit to scattering data below threshold. In this manner we presuppose that the *NN* interaction at separation radii in excess of 1 to 2 fm are established for any energy. They are the potentials from inversion of SM94 continuous fit phase shifts of which we selected to show the *pp* and *np* $T=1$ channels in Figs. 7 and 8. The inversion potentials are given in Figs. 9–11 wherein are shown the potentials of neutron-proton (solid) and proton-proton (dashed) uncoupled and coupled channels. The potentials reproduce the continuous phase shift functions in every partial wave to better than 0.02 degrees, which reflects our numerical accuracy used. The continuous energy solutions have no error bars. The single channel $T=1$ phase shifts computed from inversion potentials fit perfectly the 0 to 300 MeV energy

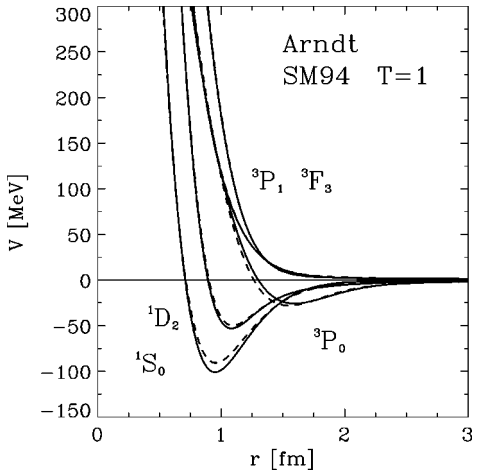

FIG. 9. The inversion potentials from the SM94 $T=1$ uncoupled channel phase shifts. The potentials from inversion of neutron-proton and proton-proton data are displayed by the solid and dashed curves, respectively.

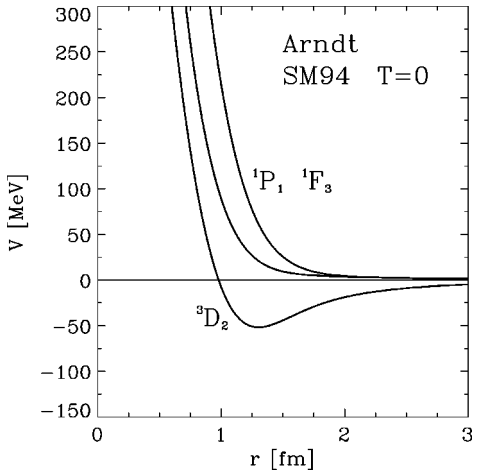

FIG. 10. The inversion potentials from the SM94 $T=0$ uncoupled channel phase shifts. The nomenclature is as in Fig. 9.

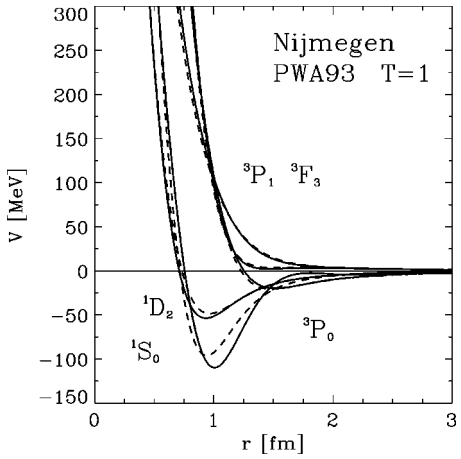

FIG. 12. The inversion potentials from the Nijmegen PWA93 $T=1$ uncoupled channel phase shifts. The nomenclature is as in Fig. 9.

region and its extrapolation to 1.6 GeV agree quite well with the real parts of the Arndt phase shifts [1]. Inherently, the extrapolation is given by the rational representation of the data which form the input to inversion with the implication that all phase functions are real and asymptotically decay $\lim_{k\to\infty}\delta(k)\sim o(1/k)$. This implies that the short-range interaction is either attractive, for phase functions which are positive and remain positive at high energy, or repulsive, for phase functions which are negative and remain negative at high energy. This choice of extrapolation permits evaluation of singular potentials with a behavior near the origin $\sim 1/r$, and which imply soft core potentials. We have regularly updated our inversion potentials and used as input the phase shift solutions PWA93 [21], VV40, VZ40, FA91, SM94, SM95, as well as several other solutions from SAID [25,31,32]. Any of these could have been used as our background, although we consider the principal set to be PWA93 from Nijmegen [21], SM94, and VZ40 from Arndt *et al.* [1]. Only PWA93 single channel results are shown in Fig. 12 as solutions to VZ40 are very similar to the potentials found using SM94 and which have been shown before. Qualitatively, the two sets of inversion potentials have the same structure but quantitatively they differ especially in the repulsive region. These differences reflect the uncertainties in the extrapolation of phase shifts to higher energies. The SM94 potentials have been chosen as background because we have used the real parts of the SM94 phase shifts in the region 300 MeV to 1.6 GeV to constrain the extrapolation. Nijmegen phase shifts do not exist above 350 MeV. Nevertheless, the high-energy constraint is weak. Now there are SM97 phase shift sets which extend to 2.5 GeV. They are qualitatively similar to the SM94 in the range 300 MeV to 1.6 GeV, and as the actual phase shifts are complex, we saw no fundamental reason to change the extrapolation based upon the SM94 solution. While the extrapolation determines how soft or hard is the core, the core radius is fixed largely from the low-energy data. The core properties of the SM94 proton-proton inversion potentials are displayed in Fig. 13. Note that the core radii of the channels differ. Also, in all channels, the potential is repulsive inside 0.8 fm. Of particular interest are the classical turning points for our investigations of scattering to 2.5 GeV. For the highest energy they are about 0.5 fm increasing to about 1 fm at low energies.

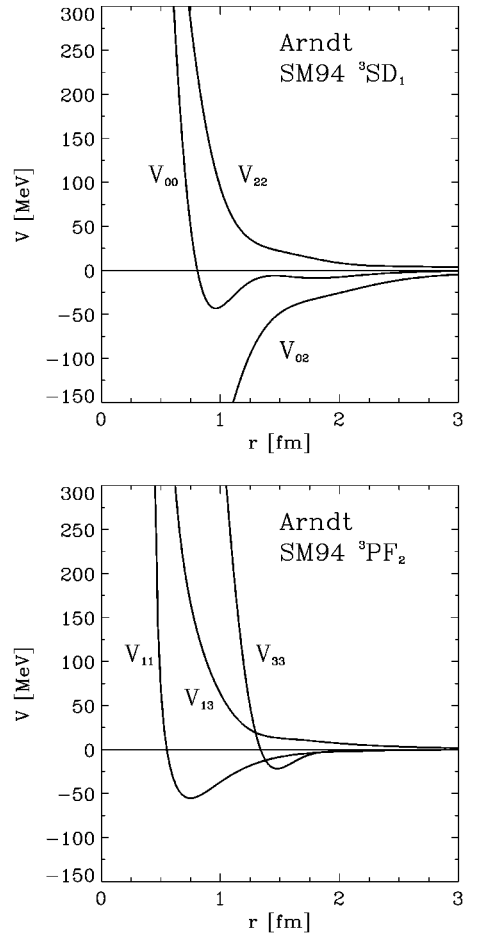

FIG. 11. The inversion potentials from the SM94 coupled np channel phase shifts. The subscripts of V_{ij} refer to the coupled orbital angular momenta, $V_{ij}(np)=V_{ij}(pp)=V_{ji}$.

With the inversion potentials as background, we used the optical potential approach to find high precision fits to the partial wave phase shifts (up to $L=6$) and for energies to 2.5 GeV. Guided by the Chou-Yang diffraction model [13,14], calculations have been made using Gaussian range values

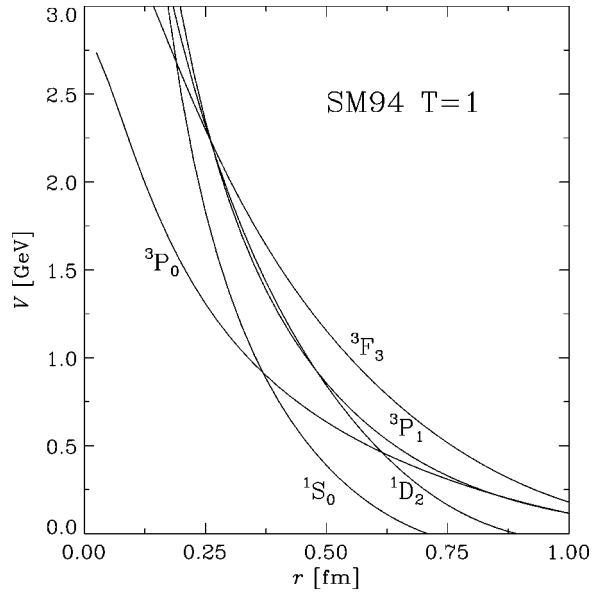

FIG. 13. The short-range properties of the proton-proton inversion potentials from the $T=1$ SM94 phase shifts.

between 0.5 and 1.2 fm which reflect the range of classical turning points in the background potentials. We show only results where the real and imaginary optical model potentials have the same range. The current analysis shows no evidence that they should differ. These values also span the radii of the little bag (0.5 fm) to the MIT bag (1.2 fm). The optical potentials strengths then were found to be smooth functions and reproduce perfectly the continuous energy fit of SM97 [18] in the full energy range 0 to 1.6 GeV for neutron-proton scattering and 0 to 2.5 GeV for proton-proton scattering. These results are depicted by the solid lines in Figs. 1–6. The results for all uncoupled channels are shown in Figs. 14 and 15, and for coupled channels in Fig. 16. The real and imaginary potential strengths are shown in the left and right panels, respectively. The results obtained from analyses of the SM97 data are portrayed by the open circles (pp data) and crosses (np data). The real and imaginary potential strengths are essentially charge independent. Considering the real parts of these potentials first, most channels have attractive real Gaussians which shifts the net repulsions inward. In contrast, up to 1.5 GeV, the $^1S_0$ and the $^3P_0$ Gaussians are small but add to the repulsive cores of the backgrounds. The strong energy variation in the $^1D_2$ and $^3F_3$ channels reflect the Δ and N^* resonance contributions to scattering; contributions that had been predicted by microscopic calculations [5]. The large strengths in these channels simply reflect centrifugal barrier shielding. The imaginary parts of the potentials also show clearly the effects of the two known resonances. These variations indicate central peak values of $\sim$625 MeV in the $^1D_2$ and $\sim$900 MeV in the $^3F_3$ channel. As the Δ and N^* have relative L with the other nucleon of 0 and 1, respectively, the resonance strengths are distributed in many partial waves so accounting for the variation in effect that they have in the channels shown explicitly in these figures. This is well understood microscopically as well. In the other uncoupled channels, with the exception of the $^3P_0$, we observe a smooth imaginary Gaussian reflecting an increased absorption with energy. The $^3P_0$ case has a maximum absorption at $\sim$1 GeV which corresponds to an invariant mass of $\sim$2.325 GeV. At this point we note that the strong variation of absorption in the $^3P_0$ potential is associated with a $0^-;T=1$ state. In addition, analysis of neutron-proton data in the $^1P_1$ channel indicate a dramatic effect above 1 GeV. Such could be associated with a $1^-;T=0$ state. Despite the resonance features discussed above, the optical potentials have very smooth strength variation in all channels. They do not reflect any specific thresholds. At the range chosen (0.7 fm for $L=0-2$, and 1 fm for $L=3-6$), all interaction strengths typically are of several hundreds of MeV with fluctuations due to the prevailing resonances. An exception is the $^1P_1$ np channel. But this channel is sensitive to fine details in partial wave analyses and is strongly correlated with the determination of the mixing angle ϵ_1. In some channels, and most clearly in the $^1S_0$, $^3P_0$, $^3P_1$, and $^1D_2$, we notice that the potential strengths have a kink at 1.75 GeV. However, as confidence in the phase shift analyses for energies above 1.6 GeV rest solely on cross-section data without spin observables, no conclusions should be drawn about these structures as of yet. We note again that, for higher partial waves, the interaction region determined from a Gaussian is shielded from the centrifugal barrier and so a much larger strength is required to achieve an effect. Such is evident in the results for the $^1G_4$, $^3H_5$, and $^1I_6$ channels and at low energies.

We have studied the range dependence of the optical models in the interval 0.5 to 1.2 fm and show the results in three-dimensional plots. In Figs. 17 and 18 the real and imaginary strengths are plotted as functions of kinetic energy and range and for the channels as indicated. Note that the real and imaginary potential ranges were kept identical in these calculations. Notably, as we expect with increasing range the potential strengths decrease. From these figures we note that, with a channel independent range of 0.7 to 0.85 fm, the optical models have evenly distributed strengths in the dominating $L=0-3$ channels, while clearly maintaining positions and widths of the known resonances. This choice of optical model geometry with evenly distributed strengths of several hundred MeV means that effective absorption (strengths from 0 to 50 MeV or more) occur for radii larger than 0.7 fm. With Gaussian forms that absorption is quite localized and, from the history of optical model studies in general, we infer that the maximum loss of flux in this case lies in a range 1 to 1.2 fm. To substantiate this claim we calculated the loss of flux from

$$\vec{\nabla}\cdot\vec{J}=\frac{i}{\hbar}(\psi^* H\psi-\psi H^*\psi^*)=-\frac{2}{\hbar}W_{OMP}(r,T_{\rm lab})|u(kr)|^2 \tag{19}$$

where the radial physical solutions $u_{SLJ}(kr)$ enter. In Fig. 19 we show this radial loss of flux for the analyzed proton-proton data and single channel partial waves, in particular the $^1D_2$ and $^3F_3$ channels. The energy interval is limited to 0.6–2 GeV, the radial domain from 0.8 to 1.4 fm is shaded to emphasize the crucial absorption region between 1 and 1.2 fm.

These conclusions have been drawn from analyses of data to 2.5 GeV. We anticipate that such will remain the case as sensitive data at higher energies are gathered and analyzed. We expect that doing so with a complex optical potential

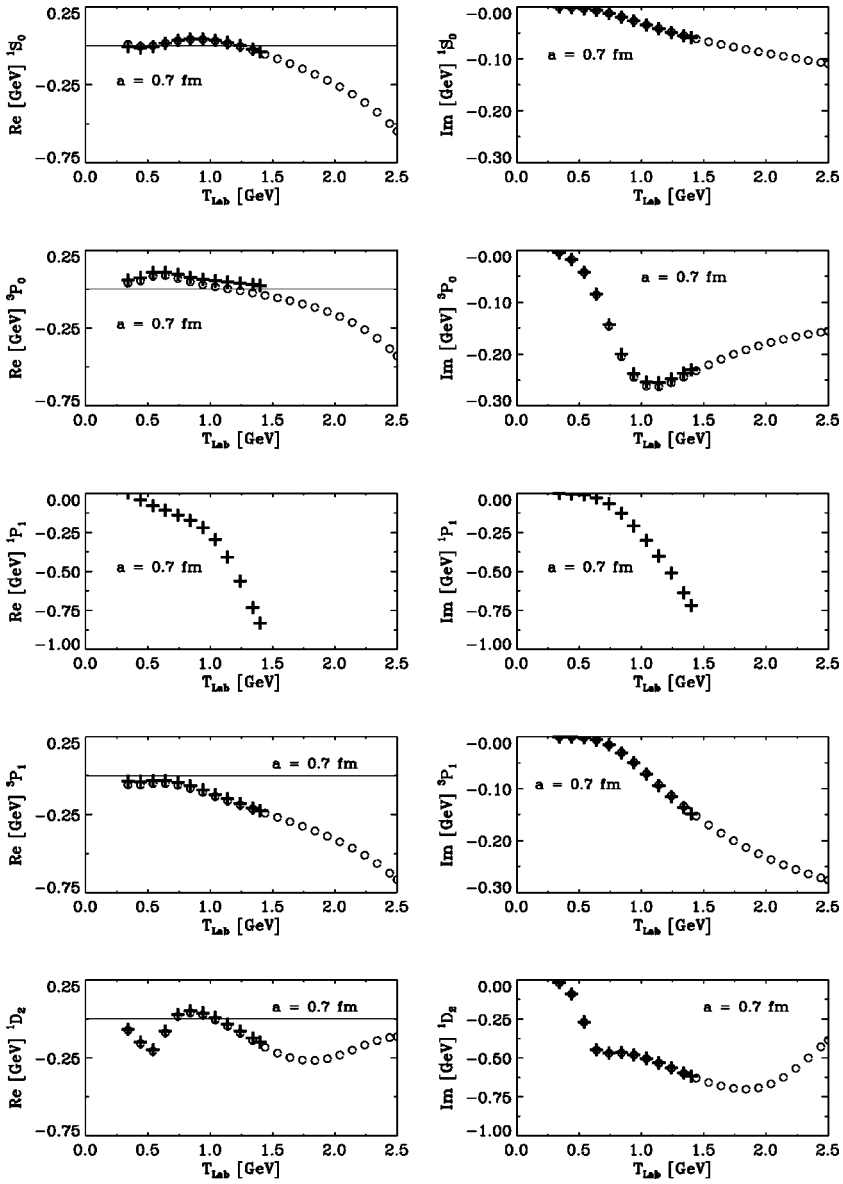

FIG. 14. The optical model potential strengths as functions of energy for Gaussian forms with range 0.7 fm for uncoupled $L=0-2$ channels. The real strengths $V_0(T_{\rm lab})$ are shown on the left and the imaginary ones $W_0(T_{\rm lab})$ on the right. The circles and crosses depict the results of our analyses of the pp data to 2.5 GeV and of the SM97 np data, respectively.

representation will result in a potential that is less channel dependent until it merges with the diffraction models of high-energy physics. Thus, presuming phase shift analyses of new data in the 1 to 5 GeV range stay consistent with the conjectures of smoothness, there is a geometric connection of NN scattering at all energies. The diffraction models are understood as the geometric realization of Regge theory with Pomeron exchange. No intrinsic structure of the nucleon is identified from that data. Such requires deep inelastic scattering studies. A consequence of the continued geometric picture then is that such intrinsic structures will not be evident in low- and medium-energy data save for the established roles of the Δ and $N^\star$ resonances. This is a picture that is consistent also with the results obtained using boundary condition models, such as the P-matrix formalism [22], and using the Moscow potential approach [30].

IV. THE GEOMETRIC PICTURE

The geometric picture we have of NN scattering can be divided in two segments: a soft and a hard part. The soft part we identify with the region outside ~ 1 fm and in which the boson exchange processes are the relevant mechanisms. The associated potential strengths do not exceed 100 MeV and are much less for most radii. The hard part encompasses the internal region (inside 1 fm) and ultimately is QCD dominated. The geometry of our optical model as well as of high-energy diffraction models place production processes in the transition region of these two. However, our view of ''soft'' is perhaps ''supersoft'' in the high-energy terminology and our view of ''hard'' in that terminology may be ''soft.''

At low energy, meson production is dominated by the processes involving intermediate resonance formation of which the Δ resonance is the most important. We consider

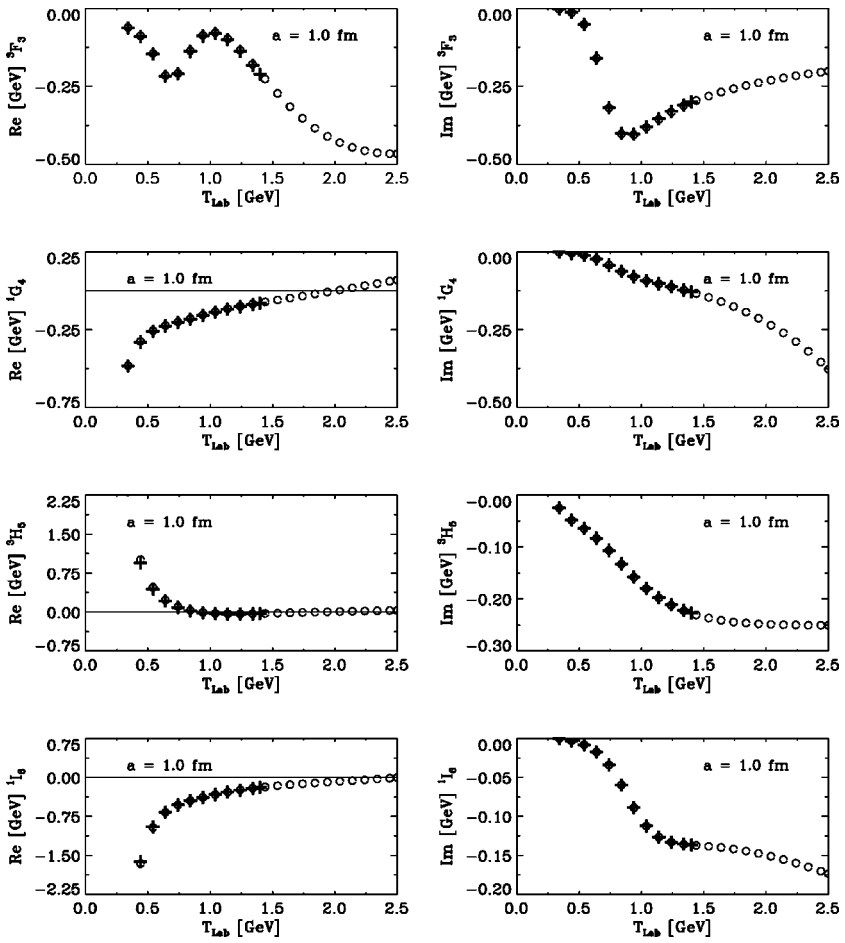

FIG. 15. Same as Fig. 14 but for the uncoupled $L=3-6$ channels and with a Gaussian range of 1.0 fm.

just the Δ at this time. There are two extreme geometric pictures for its excitation. These extremes are the result of potential model descriptions of πN scattering in the P_{33} channel found using either nonlocal (separable) interactions in momentum space or local interactions in coordinate space.

The first type of interaction is obtained by using the separable potential from the Graz group [39], by using a boson exchange model as has been done by Pearce and Jennings [40], or by using OSBEP [41]. Both boson exchange models include the Δ as an s-channel resonance whereby $\pi+N \rightarrow \Delta \rightarrow \pi+N$ is to be calculated. We have used all three interactions. The separable Graz potential, for $L=1$ πN scattering, has the form

$$V_1(k,k')=g_1(k)\lambda(s)g_1(k'), \tag{20}$$

with the form factor

$$g_1(k)=k\frac{262.675}{k^2+(1.619)^2}. \tag{21}$$

The parameter $\lambda(s)$ in general is just a number independent of s but in the resonant P_{33} channel it was required to be

$$\lambda(s)=\frac{1}{s-m_0^2} \tag{22}$$

with $m_0=1333.95$ MeV.

The second type of interaction is typified by our inversion approach [32]. With these the scattering can be interpreted as a t-channel exchange. The inversion result is a solution in coordinate space and the wave functions we seek result directly with the method. In contrast, the separable potential model and both boson exchange pictures were obtained by solving the appropriate integral equations in momentum space and then Fourier transforming into coordinate space. Thereby we obtained probability distributions in coordinate space for all interactions to allow geometric interpretation. To support our claim that the two pictures are extreme, we present in Figs. 20–23 the moduli of those coordinate space wave functions in the P_{33} πN channel as functions of the Mandelstam variable (s) in the regime of the Δ resonance. The radial distributions are very different. The boson exchange results describe a molecularlike system while the local inversion potential depicts a highly concentrated πN system where the pion and nucleon are fused. This has been a most astonishing result as our initial expectations were that the two schemes would infer that the Δ was an elementary excitation of the nucleon interpretable as a reorientation and alignment of valence quarks. Since the rms radii of both a pion and a nucleon are 0.7 and 0.8 fm, respectively, the inversion picture implies that the Δ arises with practically a full overlap of the two hadrons so that it would then have a size of a nucleon and, concomitantly, that the meson cloud of a Δ is essentially that of the nucleon. On the other hand, the results from the boson exchange models suggest that the Δ is

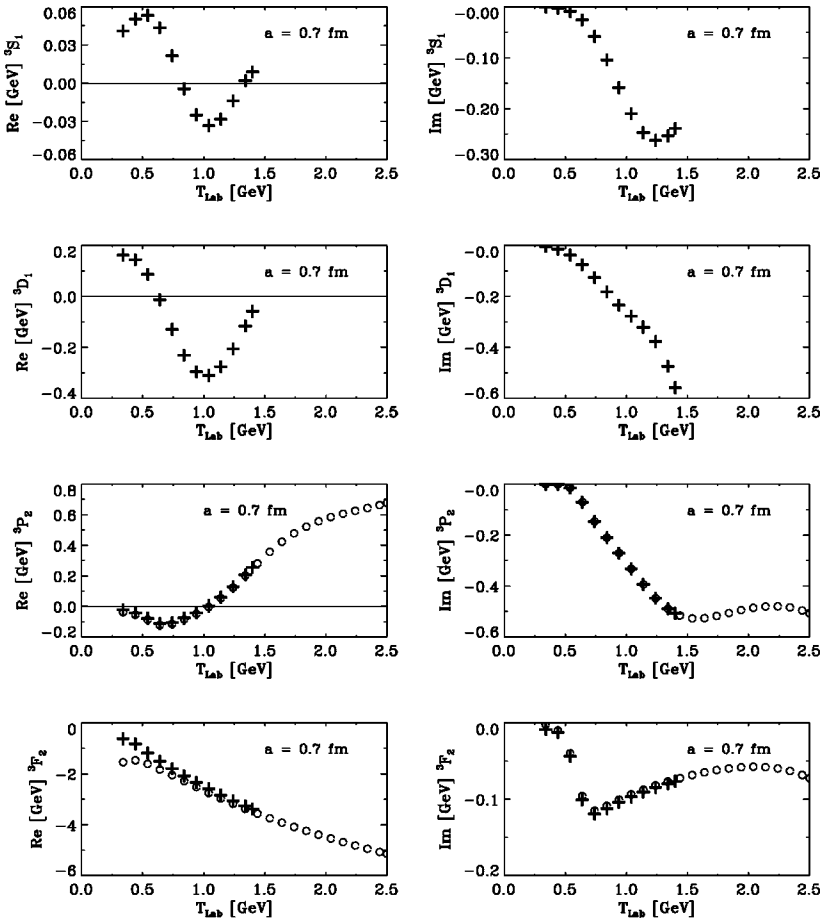

FIG. 16. Same as Fig. 14 but for the coupled channels $^3SD_1$ and $^3PF_2$. Higher partial waves have been neglected.

far more extensive implying that the meson cloud of a Δ is significantly different to that of a nucleon. We have studied this situation also for other resonances of hadronic systems and found in all cases such a difference between the radial wave functions associated with separable and inversion potentials.

The results being such a surprise led us to look at properties of other hadron-hadron scattering systems for which phase shift analyses exist to allow inversion. The inversion potentials for $\pi\pi$, πK, KN, πN, and NN have been compared [31,32] for cases where there exists low-energy resonances in $L=0-2$ partial waves. These calculations revealed two groups of short-range potentials; one class being totally repulsive, the other having a barrier inside of which is a strong attractive well. In Fig. 24 we display this geometry in a few cases, with which resonances, $\Delta=\pi N(P_{33})$, $\sigma=\pi\pi(\delta_0^0)$, and $\rho=\pi\pi(\delta_1^1)$, are associated. We understand these potentials as effective operators which appropriately describe the dynamics of the full system upon projection into the elastic channel space. In potential scattering terms then, the resonance is associated with barrier penetration into an attractive well. The α decays of heavy nuclei are classic examples of barrier penetration in nuclear physics. The usual barrier for the α decay is broad and not high. In contrast, the Δ resonance is produced by one that is very thin ~ 0.1 fm, but extremely high $\sim 2-5$ GeV. In both types of potentials, the boundary conditions on the wave functions at the origin are that the wave functions must vanish except for the $L=0$ case. The difference in establishing a resonance then lies with the matching of the internal with external wave functions at the barrier. With the extremely high and thin barrier, the dynamics of the internal system is practically decoupled from the external one. Thus we associate no dynamics with the thin barrier in contrast to the α-decay situation in which the barrier is essential in the formation dynamics of the emerging α. The πN system then comprises essentially two decoupled dynamic domains. Given the potentials we have found, this effective decoupling would hold to 2–5 GeV, above which we anticipate the strong absorption model is valid. The Δ and $N^\star$ are $L=1$ resonances and are evident as such in cross sections since the $L=1$ wave function must vanish at the origin. For $L=0$ scattering the wave functions at the origin are not constrained and so no sharp resonance effect is likely to evolve. These considerations also imply that the resonances arise with practically a full overlap of the two hadrons, so that they too would then have a size of a single hadron. There is then a consequence for NN scattering above threshold in that meson production is an emanation from the hard QCD (bag) region of one or the other nucleon, whether that be from nonresonant or resonant processes.

We do not ascribe any further physical attribute to the potentials found. Rather they are just effective local potential operators that produce wave functions at separations ~ 1 fm consistent with boundary condition models [22,11]. Concomitantly, the data from which these results have been obtained then contain no further information on substructures of the systems. We await such advances in QCD theory.

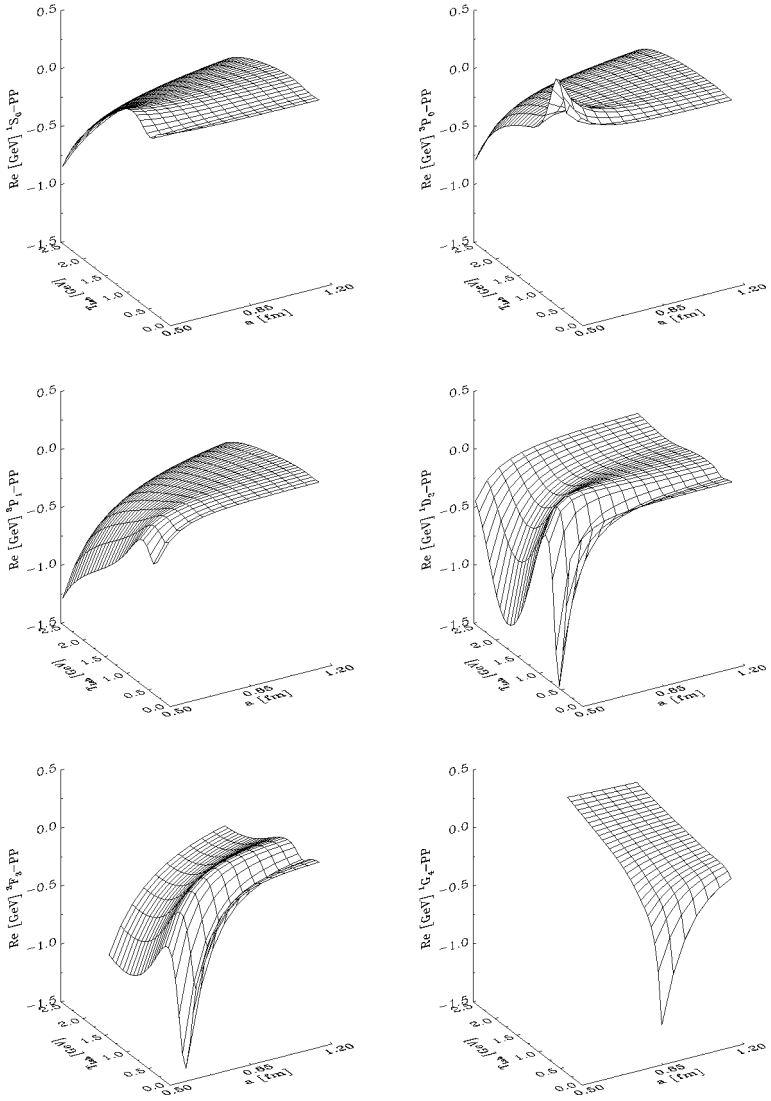

FIG. 17. The variations of the real parts of the pp optical potentials in various channels as functions of $T_{\rm lab}$ and of the range of the Gaussian form.

We restate the surprising feature of the studies that while the boson exchange models are tuned also to produce similar appropriate boundary conditions, they do so at a significant larger radius of ~ 2 fm or more. Differences such as these mean that the interpretation of results of momentum space calculations need be made carefully if those results are to be discussed from a geometric point of view. We can ask: From where are the pions produced in *NN* scattering? From our local inversion model it is clear that such must come dominantly from the hard region or QCD sector. But it is not so clear that this viewpoint can be upheld with the boson exchange models, as they are used presently, without baryon exchanges.

The formulation of a model, for example with *NN* scattering the boson exchange model, relies on *a priori* assumptions which we associate with the physics of the problem. The mathematical structure of the specific boson exchange model formulations shows a factorization of terms. But the experiments are compared with the full product of amplitudes and the results are not very sensitive to the details of any isolated process. This can be understood in terms of filter theory. To isolate physics uniquely becomes very difficult in instances where many filters determine the total result. Complicated models may reproduce an important effect by a new or just by small modifications of the other existing components of the theory. When this is so, an implication may be that different models can claim physical significance as they yield equally good fits to data. At present we have no practical and decisive experiment at hand which could discern our t-channel view from the s- and u-channel boson exchange model pictures despite the geometric interpretations put forward.

V. SUMMARY AND CONCLUSIONS

As the latest partial wave amplitude analyses of *NN* scattering data extend to 2.5 GeV and, notwithstanding known resonance effects, are very smooth functions of energy, the history of optical model approaches to data with such characteristics suggested to us that we interpret *NN* scattering from 0 to 2.5 GeV in terms of a geometric model involving local potential operators in each partial wave channel.

Below threshold, local potential operators have been deduced from high precision fits to the data. So also are mo-

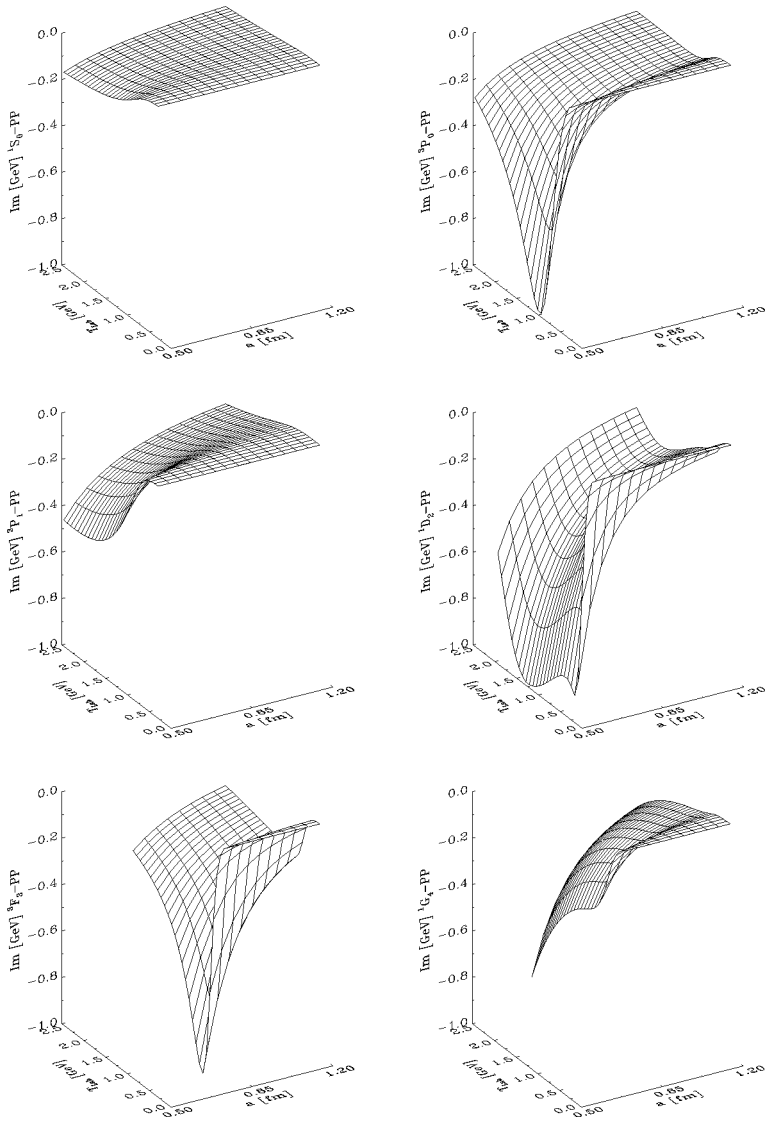

FIG. 18. Same as Fig. 17 but for the imaginary potentials.

mentum space models built upon boson exchange mechanisms. However, above threshold and with increasing energy, the semimicroscopic approaches using boson exchanges become very complex. The simplicity of an optical model approach with a complex potential to allow for pion production as flux loss from the elastic scattering channel commends itself as it is flexible in use and provides a connection between the low-energy (boson exchange) regime and the high-energy regime where essentially a black disc absorption replicates *NN* cross sections. Between the two energy regimes we place our optical model and base it upon the low-energy local potential operators as background. Any local case could be used as background for a model analysis of above threshold data. However, there are a number of reasons why we have used inversion potentials as the background in our optical model approach to *NN* scattering above threshold. First the inversion potentials are constructed so that high precision fits to partial wave phase shifts in the energy regime 0 to 300 MeV used as input in the inverse scattering theory are retained. Second, in studies made using phase shifts chosen from a model calculated set, e.g., from the Bonn or Paris interactions, the inversion potentials found are consistent with the specific properties of those semimicroscopic interactions as far as we can check. Third, semimicroscopic theories of *NN* scattering (0 to 300 MeV) give quality fits to phase shifts in most partial waves and so can be the underpinning description of physical processes for the inversion potentials. Fourth, as more data has been gathered over the years, the results of phase shift analyses vary in the precise values suggested for phase shifts in some channels, notably the $^3P_0$, and in the below threshold range (to 300 MeV) in particular. Inverse scattering theory always maps the input and so has the flexibility to be tuned to ensure, as a background for analyses of data above 300 MeV scattering, that the below threshold information currently in vogue will be exactly reproduced and maintained. Finally, by using the inversion potentials as background, whatever one may glean from the character of optical potentials found by fits to above threshold data can be assured as due to underlying processes additional to those responsible for scattering at subthreshold energies.

The optical potentials we have found are consistent with properties of scattering known from other analyses. Specifically the geometries of absorption terms are consistent with

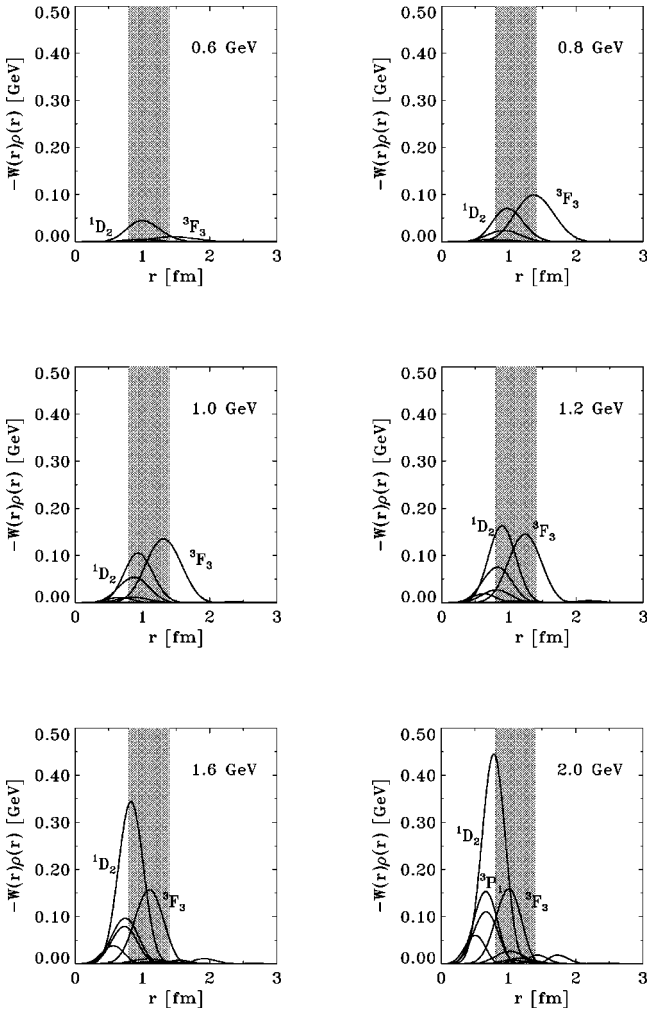

FIG. 19. Absorption of the radial probability current for important partial waves and projectile energies between 0.6 and 2 GeV. The radial range 0.8–1.4 fm is shaded.

the profile functions given by the diffraction models, and their energy variations trace the properties of the known Δ and N^* resonances. Thus meson production, reflected in the extent of the imaginary part of these optical potentials,

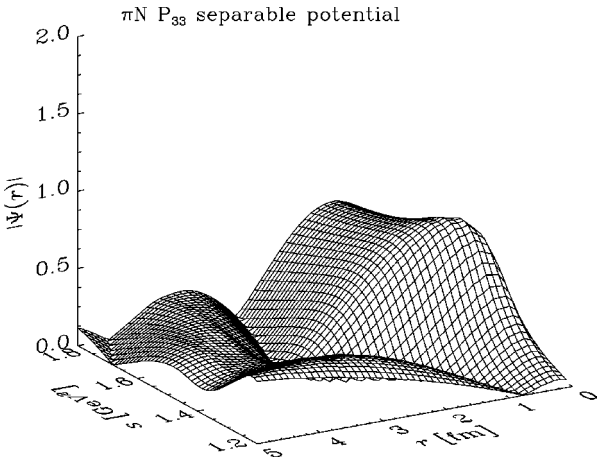

FIG. 20. The modulus of the πN wave function in the P_{33} channel of the separable interaction defined in the text in coordinate space and as a function of s.

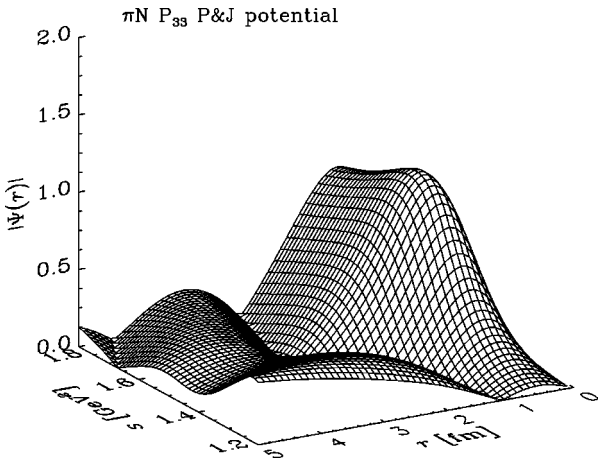

FIG. 21. Same as Fig. 20 except for the Pearce-Jennings interaction.

would arise effectively from a ''fused'' system of the colliding hadrons, and the resonance would be an object of extent similar to a nucleon. The implication then is that meson production would arise from almost complete overlap of the two colliding hadrons. This picture is consistent with what is obtained from a local interaction of πN scattering at resonance energies. The associated wave functions imply that those resonances are local objects essentially the size of a nucleon.

This view is consistent also with conclusions reached by Povh and Walcher [42] from their discussion of elastic $\bar{p}p$ scattering. They used an optical model approach to analyze cross-section data identifying annihilation processes as flux loss associated with the imaginary part of that optical potential [43]. They deduce an absorption probability in the S and P waves defined by

$$p_{\ell}^{\mathrm{abs}}(r) = W_{OMP}(r) u_{\ell}(kr) j_{\ell}(kr) r^2. \tag{23}$$

These probabilities are quite sharply peaked functions, peaking at 1–1.2 fm. Thus the absorption is quite localized. Interpreting their results in terms of physical processes means that, at very high energies, scattering is determined by quark-quark interactions with a range determined by the profile

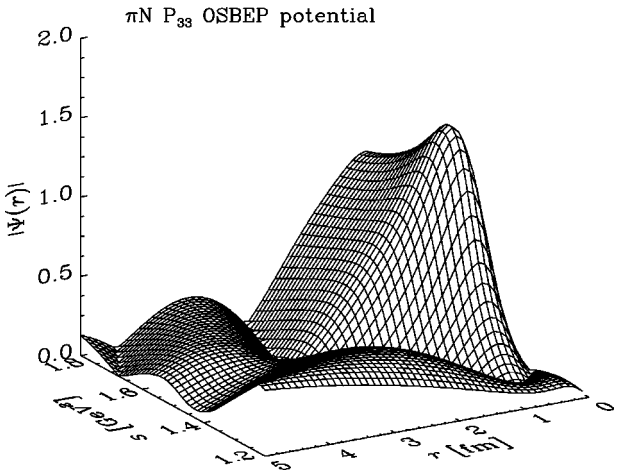

FIG. 22. Same as Fig. 20 except for the OSBEP interaction.

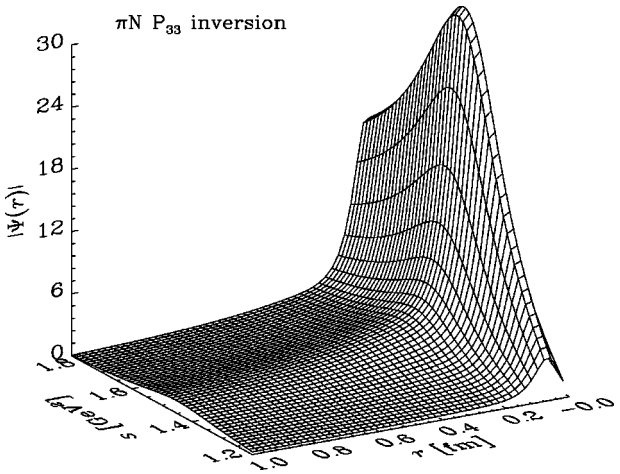

FIG. 23. Same as Fig. 20 except for the inversion interaction.

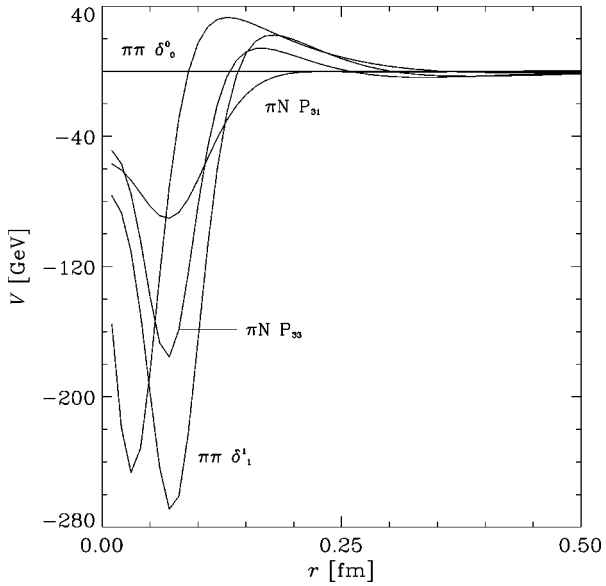

FIG. 24. The short-range potentials found by inversion of πN and $\pi\pi$ phase shift data.

function. At lower energies that quark interaction range manifests itself by the annihilation within the QCD sector of the combined $\bar{p}p$ system.

In contrast, using a separable (momentum space) model of NN scattering, similar to those of boson exchange models, leads to a Δ resonance that has a moleculelike probability distribution. The implication for pion production in NN scattering is that pions would be released from long (spatial) ranged attributes of the Δ, to wit at least in part meson production would be ''soft.'' We do note, however, that scattering in higher partial waves deals essentially only with the periphery and so meson production in those cases, if such be possible, may well be ''soft'' and involve mesons from the meson cloud.

The smooth behavior of the optical potential strengths, the reflection in those variations of the known resonance characteristics, and the consistency of the absorptive terms with the high-energy profile functions, indicate that NN elastic scattering is not sensitive to any specific QCD effect, save that such are necessary to specify intrinsic structures of the known resonances. All that seems needed to analyze the NN data is a reasonable core radius and diffuseness of the flux loss processes. We do note, however, that more NN elastic scattering data are needed to pin down with more certainty the energy variations of the partial wave scattering amplitudes so that an even more discerning view may be taken about the specific optical potential characteristics. Also more data in the forward scattering region would be desired, i.e., for low momentum transfer $0.01-0.5\ (\mathrm{GeV}/c)$, as this data would help confirm the link between our optical model and higher energy diffraction models. Finally, should perturbation calculations of small effects to scattering be of issue, the optical model would be suitable to establish distorted waves in a distorted wave approximation analysis.

ACKNOWLEDGMENTS

This work was supported in part by grants from the Forschungszentrum Jülich and the Australian Research Council. H.V.G. and K.A.A. acknowledge with gratitude the support of the University of Melbourne by means of a travel grant in aid.

[1] R. A. Arndt *et al.*, Phys. Rev. D **25**, 2011 (1982); **28**, 97 (1983); **35**, 128 (1987); **45**, 3995 (1992); Phys. Rev. C **56**, 3005 (1997).
[2] J. Bystricky, C. Lechanoine-Leluc, and F. Lehar, J. Phys. (Paris) **48**, 199 (1987); **48**, 985 (1987); **48**, 1273 (1987); **51**, 2747 (1990); C. Lechanoine-Leluc and F. Lehar, Rev. Mod. Phys. **65**, 47 (1993).
[3] F. Myhrer and J. Wroldsen, Rev. Mod. Phys. **60**, 629 (1988).
[4] R. Machleidt, Adv. Nucl. Phys. **19**, 189 (1989); R. Machleidt and G. Q. Li, Phys. Rep. **242**, 5 (1994).
[5] H. Popping, P. U. Sauer, and Xi-Zhen Zhang, Nucl. Phys. **A474**, 557 (1987); A. Bulla and P. U. Sauer, Few-Body Syst. **12**, 141 (1992).
[6] J. Dubach, W. M. Kloet, and R. R. Silbar, Nucl. Phys. **A466**, 573 (1987).
[7] Ch. Elster, W. Ferchländer, K. Holinde, D. Schütte, and R. Machleidt, Phys. Rev. C **37**, 1647 (1988); **38**, 1828 (1988).
[8] C. G. Fasano and T.-S. H. Lee, Nucl. Phys. **A513**, 442 (1990).
[9] F. Sammarruca and T. Mitzutani, Phys. Rev. C **41**, 2286 (1990).
[10] A. Valcarce *et al.*, Phys. Rev. C **49**, 1799 (1994).
[11] E. L. Lomon, Phys. Rev. D **26**, 576 (1982); P. LaFrance, E. L. Lomon, and M. Aw, nucl-th/9306026, MIT-CTP-2133; E. L. Lomon, nucl-th/9710006.
[12] P. D. Collins, *An Introduction to Regge Theory* (Cambridge University Press, Cambridge, 1977).
[13] D. F. Jackson, Rep. Prog. Phys. **37**, 55 (1974).
[14] M. Kamran, Phys. Rep. **108**, 275 (1984).
[15] A. Donnachie and P. V. Landshoff, Phys. Lett. B **387**, 637 (1996); **296**, 227 (1992).

[16] G. Matthiae, Rep. Prog. Phys. **57**, 743 (1994).
[17] V. G. Neudatchin, N. P. Yudin, Y. L. Dorodnykh, and I. T. Obukhovsky, Phys. Rev. C **43**, 2499 (1991).
[18] R. A. Arndt, C. H. Oh, I. I. Strakovsky, R. L. Workman, and F. Dohrmann, Phys. Rev. C **56**, 3005 (1997).
[19] R. A. Arndt *et al.*, SAID via telnet clsaid.phys.vt.edu, user: said (no password), or via WWW http://clsaid.phys.vt.edu
[20] D. V. Bugg, Annu. Rev. Nucl. Part. Sci. **35**, 295 (1985); Phys. Rev. C **41**, 2708 (1990).
[21] V. G. J. Stoks, R. A. M. Klomp, M. C. M. Rentmeester, and J. J. de Swart, Phys. Rev. C **48**, 792 (1993). The phase shift data are available from WWW http://nn-online.sci.kun.nl
[22] R. L. Jaffe and F. E. Low, Phys. Rev. D **19**, 2105 (1979).
[23] I. I. Starkovsky, Sov. J. Part. Nucl. **22**, 296 (1991).
[24] L. Jäde and H. V. von Geramb, Phys. Rev. C **55**, 57 (1997); **56**, 1218 (1998).
[25] H. V. von Geramb and H. Kohlhoff, in *Quantum Inversion Theory and Applications*, Vol. 427 of Lecture Notes in Physics (Springer, Berlin, 1994).
[26] M. Lacombe, B. Loiseau, J. M. Richard, R. Vinh Mau, J. Côte, P. Pirès, and R. de Tourreil, Phys. Rev. C **21**, 861 (1980).
[27] V. G. J. Stoks *et al.*, Phys. Rev. C **47**, 761 (1993); **49**, 2950 (1994); **51**, 38 (1995); **52**, 1698 (1995).
[28] R. B. Wiringa, V. G. J. Stoks, and R. Schiavilla, Phys. Rev. C **51**, 38 (1995).
[29] R. Machleidt, F. Sammaruca, and Y. Song, Phys. Rev. C **53**, 1483 (1996).
[30] V. G. Neudatchin, I. T. Obukhovskii, and Yu. F. Smirnov, Part. Nuclei **15**, 1165 (1984).
[31] M. Sander, Ph.D. thesis, University of Hamburg, 1996; *Quanteninversion und Hadron-Hadron Wechselwirkungen* (Shaker Verlag, Aachen, 1997).
[32] M. Sander and H. V. von Geramb, Phys. Rev. C **56**, 1218 (1997); Hadron-hadron and *NN* inversion potentials are available from WWW http://i04ktha.desy.de
[33] H. F. Arellano, F. A. Brieva, M. Sander, and H. V. von Geramb, Phys. Rev. C **54**, 2570 (1996).
[34] K. A. Amos, P. J. Dortmann, and S. Karataglidis, J. Phys. G **23**, 183 (1997).
[35] P. V. Landshoff and O. Nachtmann, Z. Phys. C **35**, 405 (1987).
[36] R. Blankenbecler and R. Sugar, Phys. Rev. **142**, 1051 (1966).
[37] M. H. Partovi and E. L. Lomon, Phys. Rev. D **2**, 1999 (1970).
[38] C. Itzykson and J.-B. Zuber, *Quantum Field Theory* (McGraw-Hill, New York, 1980).
[39] K. Schwarz, H. F. K. Zingl, and L. Mathelitsch, Phys. Lett. **83B**, 297 (1979); L. Mathelitsch and H. Garcilazo, Phys. Rev. C **32**, 1635 (1985).
[40] B. C. Pearce and B. K. Jennings, Nucl. Phys. **A528**, 655 (1991).
[41] L. Jäde, Phys. Rev. C **58**, 96 (1998).
[42] B. Povh and Th. Walcher, Comments Nucl. Part. Phys. **16**, 85 (1986).
[43] C. B. Dover and J. M. Richard, Phys. Rev. C **21**, 1466 (1983).